Electronic Journal of Biotechnology 31 (2018) 93–99

Contents lists available at ScienceDirect

Electronic Journal of Biotechnology

Research article

Characterization of the ligand binding of PGRP-L in half-smooth tongue sole (*Cynoglossus semilaevis*) by molecular dynamics and free energy calculation

Zisheng Wang [a,1], Qihuan Zhang [a,1], Fancui Meng [c,1], Shuai Li [b], Qiaoqin Xu [b], Zhitao Qi [a,*]

[a] Jiangsu Key Laboratory of Biochemistry and Biotechnology of Marine Wetland, Yancheng Institute of Technology, Yancheng, Jiangsu 224051, China
[b] College of Animal Sciences, Yangtze University, Jingzhou, Hubei Province 434020, China
[c] Tianjin Institute of Pharmaceutical Research, Tianjin 300193, China

ARTICLE INFO

Article history:
Received 20 July 2017
Accepted 3 October 2017
Available online 29 October 2017

Keywords:
Immune system
Inducible gene
Ligand binding
Marine teleost
MM-PBSA
PGN binding
Molecular docking
Molecular dynamics
Peptidoglycan recognition protein
Peptidoglycan
Toll-like receptors

ABSTRACT

Background: Peptidoglycan (PGN) recognition proteins (PGRPs) are important pattern recognition receptors of the host innate immune system that are involved in the immune defense against bacterial pathogens. PGRPs have been characterized in several fish species. The PGN-binding ability is important for the function of PGRPs. However, the PGRP-PGN interaction mechanism in fish remains unclear. In the present study, the 3-D model of a long PGRP of half-smooth tongue sole (*Cynoglossus semilaevis*) (csPGRP-L), a marine teleost with great economic value, was constructed through the comparative modeling method, and the key amino acids involved in the interaction with Lys-type PGNs and Dap-type PGNs were analyzed by molecular dynamics and molecular docking methods.
Results: csPGRP-L possessed a typical PGRP structure, consisting of five β-sheets and four α-helices. Molecular docking showed that the van der Waals forces had a slightly larger contribution than Coulombic interaction in the csPGRP-L-PGN complex. Moreover, the binding energies of csPGRP-L-PGNs computed by MM-PBSA method revealed that csPGRP-L might selectively bind both types of MTP-PGNs and MPP-PGNs. In addition, the binding energy of each residue of csPGRP-L was also calculated, revealing that the residues involved in the interaction with Lys-type PGNs were different from that with Dap-type PGNs.
Conclusions: The 3-D structure of csPGRP-L possessed typical PGRP structure and might selectively bind both types of MTP- and MPP-PGNs, which provided useful insights to understanding the functions of fish PGRPs.

1. Introduction

Pattern recognition receptors (PRRs) are important molecules of innate immunity that can specifically recognize conserved molecular patterns present in pathogens but absent in the host [1]. To data, a number of PRRs have been identified in teleosts, including Toll-like receptors [2], retinoic acid-inducible gene I (RIG-I)-like receptors (RLRs) [3], NOD-like receptors (NLRs) [4], C-type lectin [5], and peptidoglycan recognition proteins (PGRPs) [6].

PGRPs were first purified from the silkworm *Bombyx mori* hemolymph according to their high affinity to peptidoglycan (PGN), the essential cell wall component of almost all bacteria [7]. Then, PGRPs were identified from several invertebrates and vertebrates. Depending on the length of their amino acids, PGRPs were divided into three types: short PGRPs (PGRP-S), long PGRPs (PGRP-L), and intermediate PGRPs (PGRP-I). The short and long PGRPs are present in all species, while intermediate PGRPs were only reported in mammals [6].

All the PGRPs possess at least one conserved PGRP domain at their N-terminals, which is approximately 160 amino acids in length. Structurally, PGRPs are similar to type 2 bacteriophage amidases, containing three peripheral α-helices and several central β-sheet strands [6]. The front face of the PGRPs form a PGN-binding groove, and many amino acid residues that are important for the functioning of PGRPs are found in this groove [8]. However, different PGRPs exhibit different PGN-binding ability toward Lys-PGN and Dap-PGN. For example, *Drosophila* PGRP-SA could bind Lys-PGN [9], while PGRP-LC and PGRP-LE bind Dap-PGN [10]. Similar results were also found in mammalian PGRPs. Human PGLYRP1 could bind Lys-PGN and Dap-PGN [11], while PGLYRP3 only bind Lys-PGN [12]. Structural

* Corresponding author.
E-mail address: qzt_wh2002@163.com (Z. Qi).
[1] These authors contributed equally to this paper.
Peer review under responsibility of Pontificia Universidad Católica de Valparaíso.

https://doi.org/10.1016/j.ejbt.2017.10.010

analysis of PGRPs provide solid basis for fully understanding the specific mechanism for PGRPs binding different PGNs.

Fish are lower vertebrates inhabiting the aquatic environment and serving as an essential link to early vertebrate evolution. It had been found that fish might possess a more complex immune system than previously believed [13,14]. To date, PGRPs have been identified in several fish species, such as zebrafish [15], grass carp [16], and rainbow trout [17]. Fish PGRPs have PGN-binding ability, amidase activity, and direct bactericidal activity [15,16,17]. However, the molecular basis for the interaction between fish PGRPs and PGNs remain unclear.

Homology modeling method is a convenient method for constructing an atomic resolution model of the protein from its amino acid sequence and an experimental 3-D structure of a related homologous protein. Using this method, the structures of many important immune molecules, e.g., interleukin (IL)-22 [18] and nucleotide binding and oligomerization domain (NOD) 2 [19], had been constructed, and the interactions with their ligands were also elucidated.

In the present study, the 3-D structure of a long PGRP from half-smooth tongue sole (*Cynoglossus semilaevis*) (csPGRP-L), a marine teleost with great economic value in China and other Asian countries [20], was constructed using the comparative modeling method. The molecular interaction between csPGRP-L and PGNs were studied using molecular docking, molecular dynamics (MD) simulations, and molecular mechanics/Poisson Boltzmann surface area (MM/PBSA) methods. This study elucidates the structural and dynamics properties of csPGRP-L and the molecular basis for csPGRP-L-PGN complex, giving first insights into the PGRP-PGN interaction mechanism in teleosts.

2. Materials and methods

2.1. Homology modeling and MD analysis of csPGRP-L

The crystal structures of human peptidoglycan recognition protein PGRP-S (PDB code: 1YCK) was selected as the template protein to build the structure of csPGRP-L. Homology modeling was performed using the Prime module of Schrödinger software [21]. Ramachandran plot was used to test the reliability of the structure.

The MD simulation system of csPGRP-L was built and run using GROMACS package 5.1 using AMBER99SB force field [22]. The amino groups were fully protonated (Lys, Arg, and N-terminal), and the carboxylic groups were deprotonated (Asp, Glu, and C-terminal). The protein was placed in a cubic box whose surface to the closest atom of the solute was set to 1.2 nm. Subsequently, TIP3P water molecules were filled in the box, and the system was neutralized with 0.10 M NaCl. The obtained system was first energy minimized using the steepest descent algorithm to remove steric clash. Then, 200 ps NVT (constant temperature, constant volume ensemble) and 500 ps NPT (constant temperature, constant pressure ensemble) MD simulations were carried out with position restrictions on protein successively. Finally, the production MD was run for 30 ns at 300 K using the V-rescale method. The pressure was kept at 1 atm using a Parrinello-Rahman barostat. Long-range electrostatic interaction was considered using the particle mesh Ewald method. Trajectories were saved every 20 ps. The final structure was extracted and used for further docking calculations.

2.2. Molecular docking of PGN ligands with csPGRP-L

The minimized structure of csPGRP-L from MD simulation was adopted as receptor. The binding site was identified using SiteMap module [23], and the receptor grid was generated using the obtained binding site with a box size of 20 Å. The ligand structures of muramyl tripeptide (MTP), muramyl tetrapeptide (MTrP), and muramyl pentapeptide (MPP) were taken from PDB databank (PDB ID: 1TWQ, 4KNL, and 2APH, respectively). The lysine residues at the third position were replaced with Dap using Maestro build tools. The structures of ligands were prepared using the LigPrep module [24]. The possible ionization state at pH 7.0 ± 2.0 was determined using the Epik method. The OPLS-2005 forcefield was used to produce the low-energy conformer. Molecular docking calculations were carried out using the Glide module of Schrödinger software at standard precision [25].

2.3. Binding free energy calculation

Six csPGRP-L-PGN complexes obtained by molecular docking were used as the initial structures for MD simulations. The topology parameters of ligands were derived using the RESP (Restrained

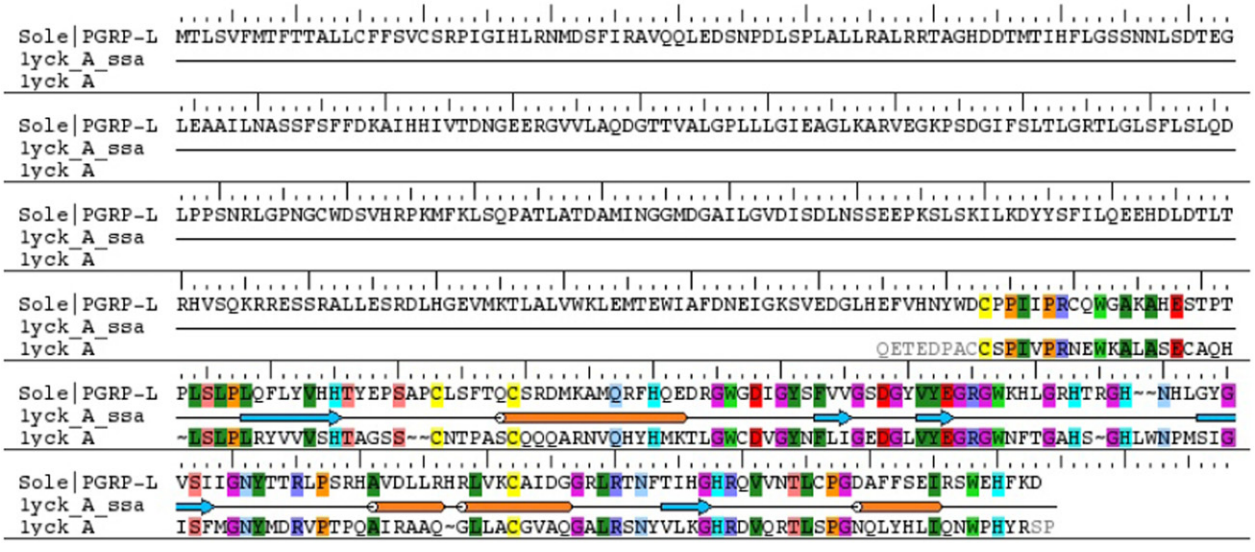

Fig. 1. Sequence alignment of LPGPR with the template PDB 1YCK.

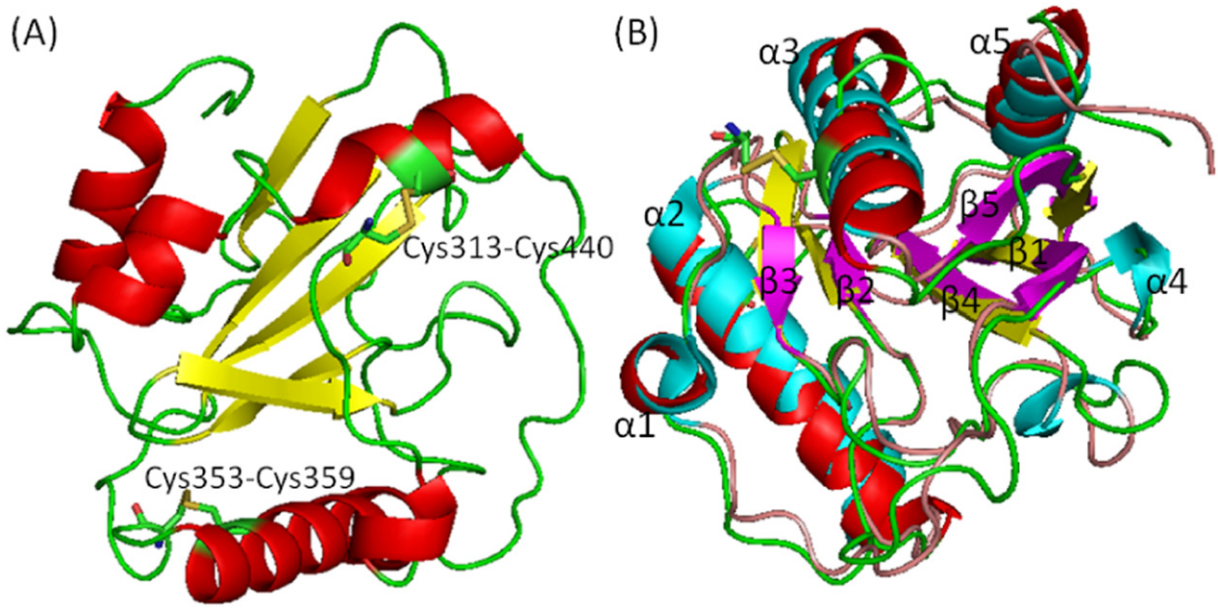

Fig 2. (A) Cartoon presentation of final structure of csPGRP-L after 30-ns MD; (B) the superposition of LPGRP with its template 1YCK. Cysteine residues that form disulfide bonds are shown in stick model. The helices, sheets, and loops are colored in red, yellow and green for csPGRP-L and in cyan, purple, and wheat for LPGRP for 1YCK, respectively.

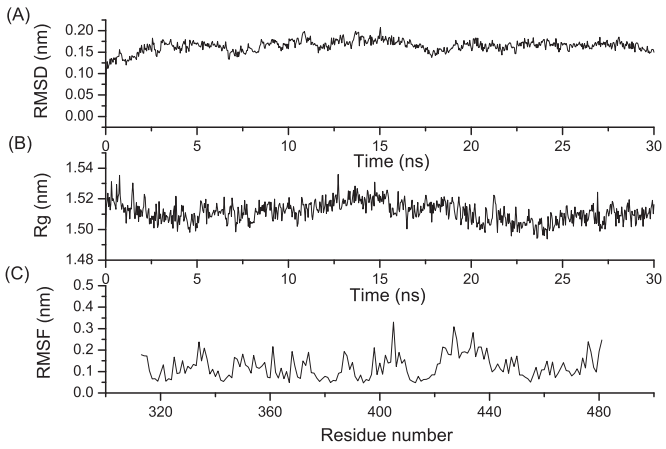

Fig. 3. Stability parameters of csPGRP-L model through 30-ns MD simulation. (A) RMSD of Cα atoms, (B) radius of gyration of csPGRP-L, and (C) RMSF of each amino acid residue of csPGRP-L.

ElectroStatic Potential) method with General Amber Force Field. The calculation steps and parameter setup were the same as that of csPGRP-L calculation. Production of MD simulation lasting for 20 ns were performed for each complex. The binding free energies between PGN fragments and csPGRP-L were calculated using the MM/PBSA method. MM-PBSA calculations were performed on the last 5-ns trajectories by using g_mmpbsa tool embedded in GROMACS software [26]. The selected nonpolar solvation model is based on the solvent-accessible surface area (SASA) with probe radius 1.4 Å.

3. Results and discussion

3.1. Structure construction of csPGRP-L

The sequence alignment of csPGRP-L with the template protein is shown in Fig. 1. 1YCK was the experimental structure of human PGLYRP1 [12]. Both 1YCK and csPGRP-L contained one PGRP domain at their C-terminal (313–481 aa), which was essential for PGN binding [27]. Thus, only residues 313~481 were constructed using 1YCK as the template protein.

It was found that all PGRPs consisted of multiple α-helices and β-sheet structures. For example, human PGRP-Iα and camel PGRP-S contain five β-strands and three α-helices [12,28], whereas *Drosophila* PGRP-SD contains six β-strands and three α-helices [29]. In this study, we found that csPGRP-L consisted of five β-strands and four α-helices, similar to that of the template protein (Fig. 2A). However, there were some differences between csPGRP-L and its template protein. The α3 helix of csPGRP-L was not preserved well and was broken in the middle of the range. Compared to its template, the β2 and β3 of csPGRP-L were obviously elongated, while β1 and β5 of csPGRP-L were shortened, and the bent region between them disappeared. In addition, α4 of 1YCK was absent from csPGRP-L. Furthermore, only two disulfide bonds were found in csPGRP-L (Cys313-Cys440 and Cys353-Cys359), and three disulfide bonds were present in the template protein (Fig. 2B).

Table 1
Docking results of PGN ligands with csPGRP-L.

	glide g-score	glide evdw	glide ecoul	glide energy	glide ligand efficiency	H-bond
MTP-Lys	−8.88	−40.66	−32.33	−72.99	−0.21	7(His345,Thr346,Glu348,Asp362,Tyr385,Arg402,His456)
MTrP-Lys	−7.52	−40.37	−37.20	−77.57	−0.16	10(His344,Glu348,Asp362,His370,Glu372,Asp373,Tyr381,His403,His456,Thr462)
MPP-Lys	−8.20	−42.45	−28.44	−70.89	−0.15	5(His344,His347,Asp362,His370,His403)
MTP-dap	−7.44	−42.32	−29.28	−71.60	−0.16	5(His344,Glu348,His370,Asp373,His403)
MTrP-dap	−7.65	−44.92	−26.49	−71.41	−0.15	6(His344,Asp362,His370,Asp373,His403)
MPP-dap	−6.77	−44.17	−21.34	−65.51	−0.12	6(Tyr347,Glu348,Asp373,Tyr381,His456)

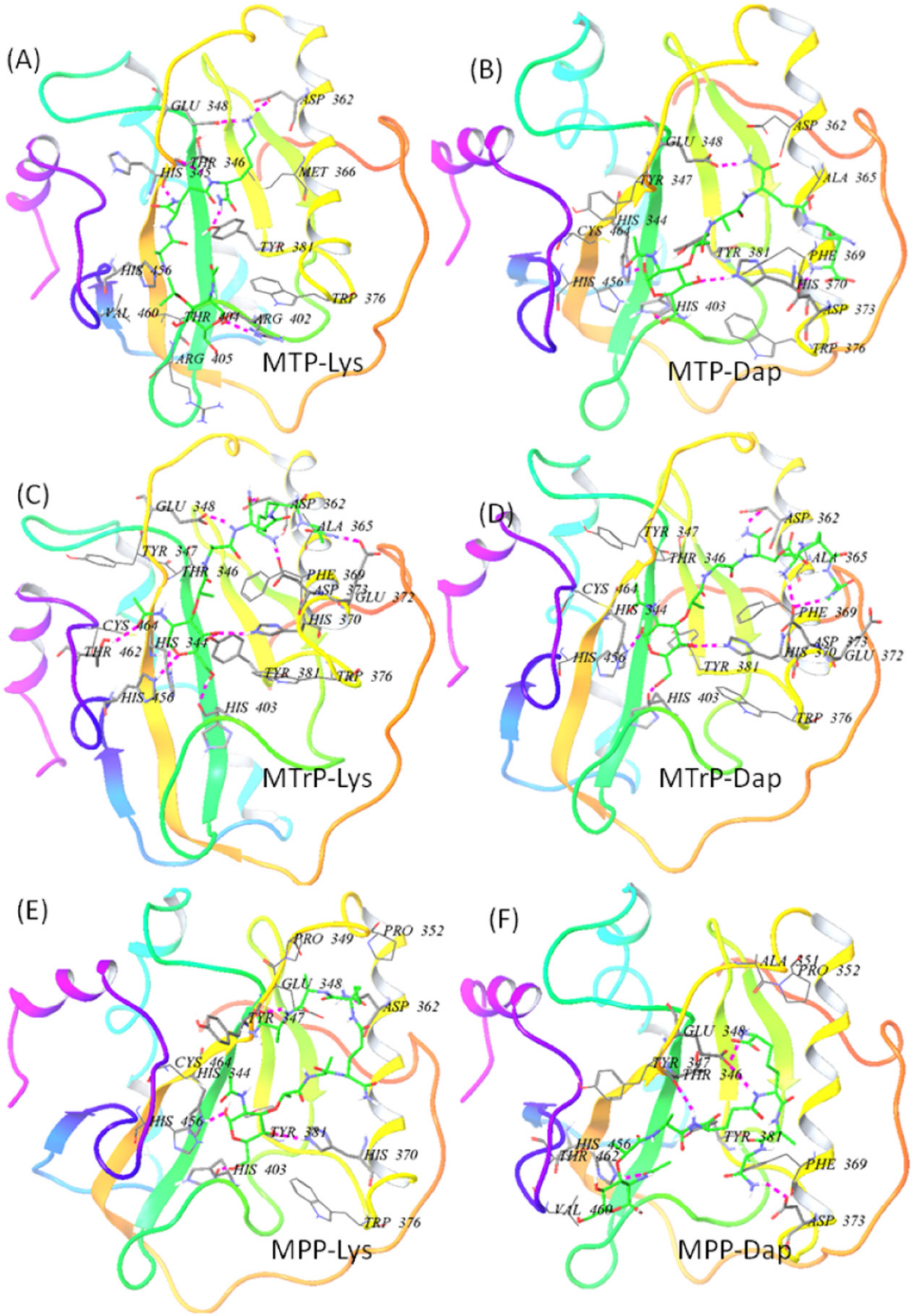

Fig. 4. Docking poses of PGN fragments with csPGRP-L receptor. (A), (C), and (E) are the interactions between Lys-type PGNs and csPGRP-L, while (B), (D), and (F) are those between Dap-type PGN and csPGRP-L. The ligands are shown in green carbon scheme and residues are shown in gray carbon scheme. Hydrogen bonds are shown as purple dotted lines.

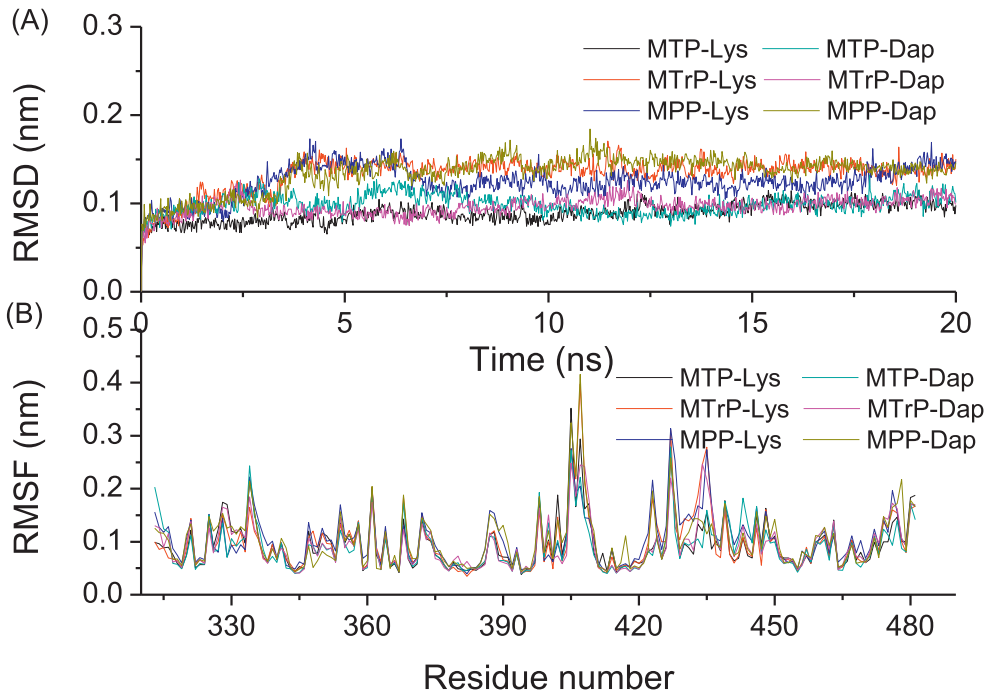

Fig 5. Stability parameters of PGN-csPGRP-L complexes. (A) RMSD of backbone atoms and (B) RMSF of amino acid residues.

The obtained structures were validated by Ramachandran plot (Fig. S1), and the result showed that most of the residues occurred in the favored or allowed regions and that only two residues (Asn408 and Arg434) appeared in the disallowed region. This indicated that our built models were reasonable and could be used for further analysis.

Fig. 3 shows the stability parameters of csPGRP-L; it can be seen that the RMSD values of csPGRP-L model increased rapidly to 0.16 nm and then fluctuated around it. The fluctuation became steady after 20-ns MD, suggesting that the system was equilibrated. Radius of gyration analysis presented an average Rg value of 1.51 nm, and the fluctuation ranged from 1.5 to 1.53 nm, revealing a good equilibration for the csPGRP-L model. RMSF analysis showed that most of the residues had a value less than 0.2 nm, except the loop regions and the C-terminal. The N-terminal region did not display a large RMSF value, which was due to the disulfide bond formed by the CYS313 and Cys440. All these analyses indicated that the csPGRP-L model was well equilibrated during the 30-ns MD simulation.

3.2. Molecular docking of PGN fragments with csPGRP-L

Molecular docking calculations were performed between PGN fragments and csPGRP-L. The docking results are presented in Table 1, and the binding modes are shown in Fig. 4. The docking score of Lys-type PGN was lower than that of its corresponding Dap-type PGN, except for MTrP. MTrP-Lys and MTrP-Dap had similar docking scores. The binding poses of Lys- and Dap-type muramyl peptides were in an extended conformation at the deep end of the binding cleft and were well in agreement with previous studies [27,30]. For the six PGN-csPGRP-L complexes, van der Waals interaction was stronger than Coulombic interaction and dominated in the whole interaction. All these PGN fragments created 5 to 10 hydrogen bonds with csPGRP-L. Residues that most frequently participated in hydrogen bond formation were His 344, Glu348, Asp373, and His 403, which formed the floor of the binding cleft. The glucose rings of MTP-dap, MTrP-Lys, MTrP-Dap, and MPP-Lys had similar binding modes with csPGRP-L, and the three hydroxyl groups of glucose rings formed three hydrogen bonds with His344, His370, and His403. Three hydrogen bonds were also observed between the muramyl moiety and human PGRP-Iα [12]. The Lys residues in MTP-Lys and MPP-Lys directed to Glu348 and Asp362, while that in MTrP-Lys faced Asp373. The amino cations of MTP-Dap and MTrP-Dap faced Asp373, while that of MPP-Dap faced Glu348. These results revealed that Glu348 and Asp362 might play important roles in the csPGRP-L selective binding to Lys-PGN and Dap-PGN. Our results also revealed that csPGRP-L might bind both types of PGNs. Similar results were also observed in other fish species, e.g., grass carp PGRP6 could bind Lys-type PGNs and Dap-type PGNs [16].

3.3. MD simulations of PGN-csPGRP-L complexes

The RMSDs of backbone atoms over simulation time for PGN-csPGRP-L complexes are shown in Fig. 5. The MTrP-Lys, MPP-Lys,

Table 2
MM-PBSA values (binding free energies) of various PGN complexes.

	Polar energies		Non-polar energies		Binding energy
	Electrostatic	Polar solvation	Van der Waals	SASA	
MTP-Lys	−82.15 ± 35.62	255.35 ± 23.75	−184.35 ± 17.17	−22.61 ± 1.40	−33.76 ± 24.71
MTrp-Lys	78.97 ± 57.41	94.32 ± 52.30	−146.80 ± 57.75	−16.43 ± 6.46	10.07 ± 60.21
MPP-Lys	−44.39 ± 90.05	170.50 ± 117.48	−131.76 ± 98.45	−15.73 ± 11.74	−21.37 ± 81.58
MTP-Dap	−13.80 ± 67.36	6.50 ± 67.77	−7.41 ± 34.58	−0.83 ± 4.42	−15.53 ± 41.77
MTrp-Dap	−28.02 ± 69.92	58.05 ± 76.82	−22.85 ± 58.15	−2.76 ± 6.94	4.42 ± 62.16
MPP-Dap	−248.42 ± 21.08	244.95 ± 14.71	−221.89 ± 15.27	−22.91 ± 1.44	−248.28 ± 19.58

and MPP-Dap displayed larger deviation than other PGNs. The RMSD rapidly increases to 0.15 nm at 4 ns, then fluctuated, and, finally, equilibrated at approximately 15 ns. The RMSD of the other three PGN complexes showed relative plateau with a slight backbone deviation of less than 0.1 nm. All residues had a RMSF value of less than 0.3 nm except residues 405 and 407, which were located at the loop region between β3 and β4. All the above indicated that all these PGN-csPGRP-L complexes were well equilibrated during MD simulations.

3.4. Binding free energies of PGN-csPGRP-L complexes

The binding free energies between PGN fragments and csPGRP-L model were calculated using the MM-PBSA method. Table 2 lists the calculated energy terms including electrostatic, van der Waals, polar solvation, and SASA energies and the whole binding free energies. It could be seen that in PGN and csPGRP-L interaction, van der Waals and SASA were negative and polar salvation terms were positive for all PGN complexes. That is, van der Waals and SASA favored the binding, while the polar salvation terms opposed the binding. The electrostatic energy was calculated to be positive for MTrP-Lys complex, while it was negative for other PGN complexes, resulting from the poor binding free energy of MTrP-Lys complex.

Our results confirmed that van der Waals interaction was the predominant contributor to the whole free binding energy for all the complexes, which was considered the most significant interaction between PGNs and receptors and might be crucial for PGN fragment recognition. Similar results were also observed in human PGRP1 [10] and buffalo PGRP1 [30]. It was noteworthy that both MTrP-Lys and MTrP-Dap had positive binding energies, while the binding energies of the other PGN complexes were all negative. This indicated that csPGRP-L could bind both types of MTP and MPP, revealing that csPGRP-L might selectively bind MTP and MPP PGNs.

To further investigate which residues of csPGRP-L played key roles in the binding of PGN, the binding interaction energies were decomposed to each residue, and the results are listed in Table S1 and Table S2. It was evident that the Dap- and Lys-type PGNs had different residue contributions. Regarding the Lys-type PGN complexes, the acidic residues Glu328, Glu348, Asp362, Glu372, Asp373, Asp378, Asp388, Glu393, and Asp481 of csPGRP-L were involved in the attraction interaction to stabilize the complexes (Table S1), while the basic residues Arg319, Lys325, Arg361, Lys364, Arg368, Arg374, Arg395, Arg402, and Arg405 contributed to the repulsion interaction to oppose the binding (Table S2). The absolute values of residue contributions for Lys-type PGN complexes were much larger than those for Dap-type PGNs complexes, and the stronger stabilization energy and destabilization energy counteracted each other. Unlike the Lys-type PGNs, Dap-type PGNs interacted with a variety of residues, among which Thr346, Arg361, and Phe369 participated in the attraction interactions for all the three Dap-type PGNs (Table S1). Phe369 was the most important residue that contributed −0.75, −2.22, and −8.55 kJ/mol to the whole binding energy for MTP-Dap, MTrp-Dap, and MPP-Dap complexes, respectively. It was found that Asn236 and Phe237 are important residues for the ability of some mammalian PGRPs to discriminate between Lys- and Dap-type PGNs [11,12,27]. Phe369 of csPGRP-L corresponds to Phe237 of mammalian PGRPs. Thus, we assumed that fish PGRPs have similar amino acid residues as mammalian PGRPs for determining the selective binding of Lys- and Dap-PGN.

4. Conclusions

In the present study, the 3-D model of csPGRP-L was constructed, and the key amino acids involved in interacting with Lys- and Dap-type PGNs were analyzed in detail. Results revealed that csPGRP-L possessed a typical PGRP structure of five β-sheets and four α-helices. Molecular docking revealed that the van der Waals interaction provided slightly larger contribution than Coulombic interaction in the PGRP-L-PGN complex. Moreover, the binding energies of csPGRP-L-PGNs computed by the MM-PBSA method revealed that csPGRP-L might selectively bind both types of MTP and MPP. Furthermore, the binding energy of each residue of csPGRP-L was also calculated, which revealed that the residues involved in the interaction of Lys-type were different from that of the corresponding Dap-type. Of course, we have to admit that our results were obtained by theoretical computing method, which needs further experimental study to be confirmed. Our study provided useful information to understand the potential functions of vertebrate PGRPs.

Supplementary material

Supplementary data to this article can be found online at https://doi.org/10.1016/j.ejbt.2017.10.010.

Conflicts of interests

The authors declare that they have no competing interests.

Financial support

This work was supported by the National Natural Science Foundation of China (Grant no. 31302221, 31272666 and 31470130) and Jiangsu Province (Grant no. BK2011418 and BK20151297) and partially by the “Qinglan” project of Jiangsu province of China and Opening Project of Jiangsu Key Laboratory of Biochemistry and Biotechnology of Marine Wetland (Grant no. K2016-08).

References

[1] Kurata S. Peptidoglycan recognition proteins in *Drosophila* immunity. Dev Comp Immunol 2014;42(1):36–41. https://doi.org/10.1016/j.dci.2013.06.006.
[2] Wei Y, Hu S, Sun B, et al. Molecular cloning and expression analysis of toll-like receptor genes (TLR7, TLR8 and TLR9) of golden pompano (*Trachinotus ovatus*). Fish Shellfish Immunol 2017;63:270–6. https://doi.org/10.1016/j.fsi.2017.02.026.
[3] Chen SN, Zou PF, Nie P. Retinoic acid-inducible gene I (RIG-I)-like receptors (RLRs) in fish: Current knowledge and future perspectives. Immunology 2017;151(1):16–25. https://doi.org/10.1111/imm.12714.
[4] Thanasaksiri K, Hirono I, Kondo H. Molecular cloning and expression analysis of NOD-like receptor 5 in Japanese flounder (*Paralichthys olivaceus*) after injection with two different formalin-killed pathogenic bacteria and poly (I:C). Dev Comp Immunol 2017;67:481–4. https://doi.org/10.1016/j.dci.2016.08.017.
[5] Liu Y, Li NQ, Zhao XP, et al. A C-type lectin that inhibits bacterial infection and facilitates viral invasion in black rockfish, *Sebastes schlegelii*. Fish Shellfish Immunol 2016;57:309–17. https://doi.org/10.1016/j.fsi.2016.08.053.
[6] Dziarski R. Peptidoglycan recognition proteins (PGRPs). Mol Immunol 2004;40(12):877–86. https://doi.org/10.1074/jbc.271.23.13854.
[7] Yoshida H, Kinoshita K, Ashida M. Purification of a peptidoglycan recognition protein from hemolymph of the silkworm, *Bombyx mori*. J Biol Chem 1996;271(23):13854–60. https://doi.org/10.1074/jbc.271.23.13854.
[8] Dziarski R, Gupta D. The peptidoglycan recognition proteins (PGRPs). Genome Biol 2006;7:232. https://doi.org/10.1186/gb-2006-7-8-232.
[9] Michel T, Reichhart JM, Hoffmann JA, et al. *Drosophila* toll is activated by gram-positive bacteria through a circulating peptidoglycan recognition protein. Nature 2001;414:756–9. https://doi.org/10.1038/414756a.
[10] Lim JH, Kim MS, Kim HE, et al. Structural basis for preferential recognition of diaminopimelic acid-type peptidoglycan by a subset of peptidoglycan recognition proteins. J Biol Chem 2006;281:8286–95. https://doi.org/10.1074/jbc.m513030200.
[11] Cho JH, Fraser IP, Fukase K, et al. Human peptidoglycan recognition protein S is an effector of neutrophil-mediated innate immunity. Blood 2005;106:2551–8. https://doi.org/10.1182/blood-2005-02-0530.
[12] Guan RJ, Roychowdhury A, Ember B, et al. Structural basis for peptidoglycan binding by peptidoglycan recognition proteins. Proc Natl Acad Sci U S A 2004;101(49):17168–73. https://doi.org/10.1073/pnas.0407856101.
[13] Venkatesh B. Evolution and diversity of fish genomes. Curr Opin Genet Dev 2003;13(6):588–92. https://doi.org/10.1016/j.gde.2003.09.001.
[14] Xiang LX, He D, Dong WR, et al. Deep sequencing-based transcriptome profiling analysis of bacteria-challenged *Lateolabrax japonicus* reveals insight into the immune relevant genes in marine fish. BMC Genomics 2010;11:472. https://doi.org/10.1186/1471-2164-11-472.
[15] Li X, Wang S, Qi J, et al. Zebrafish peptidoglycan recognition proteins are bactericidal amidases essential for defense against bacterial infections. Immunity 2007;27(3):518–29. https://doi.org/10.1016/j.immuni.2007.07.020.

[16] Li JH, Yu ZL, Xue NN, et al. Molecular cloning and functional characterization of peptidoglycan recognition protein 6 in grass carp *Ctenopharyngodon idella*. Dev Comp Immunol 2014;42(2):244–55. https://doi.org/10.1016/j.dci.2013.09.014.
[17] Jang JH, Kim H, Jang MJ, et al. PGRP negatively regulates NOD-mediated cytokine production in rainbow trout liver cells. Sci Rep 2016;6:39344. https://doi.org/10.1038/srep39344.
[18] Qi ZT, Shi RW, Li SY, et al. 3-D modeling and molecular dynamics simulation of interleukin-22 from the soi-ny mullet, *Liza haematocheila*. Electron J Biotechnol 2013;16:1–9. https://doi.org/10.2225/vol16-issue4-fulltext-3.
[19] Maharana J, Patra MC, De Chandra B, et al. Structural insights into the MDP binding and CARD-CARD interaction in zebrafish (*Danio rerio*) NOD2: A molecular dynamics approach. J Mol Recognit 2014;27(5):260–75. https://doi.org/10.1002/jmr.2357.
[20] Song W, Li Y, Zhao Y, et al. Construction of a high-density microsatellite genetic linkage map and mapping of sexual and growth-related traits in half-smooth tongue sole (*Cynoglossus semilaevis*). PLoS One 2012;8(5):e52097. https://doi.org/10.1371/journal.pone.0052097.
[21] Prime, version 9.7. New York, NY: Schrödinger, LLC; 2009.
[22] Abraham MJ, Murtola T, Schulz R, et al. GROMACS: high performance molecular simulations through muti-level parallelism from laptops to supercomputers. SoftwareX 2015;1-2:19–25. https://doi.org/10.1016/j.softx.2015.06.001.
[23] SiteMap, version 2.3. New York, NY: Schrödinger, LLC; 2009.
[24] LigPrep, version 2.3. New York, NY: Schrödinger, LLC; 2009.
[25] Glide, version 5.5. New York, NY: Schrödinger, LLC; 2009.
[26] Kumari R, Kumar R, Lynn A. g_mmpbsa-A GROMACS tool for high-throughput MM-PBSA calculations. J Chem Inf Model 2014;54(7):1951–62. https://doi.org/10.1021/ci500020m.
[27] Guan R, Wang Q, Sundberg EJ, et al. Crystal structure of human peptidoglycan recognition protein S (PGRP-S) at 1.70 Å resolution. J Mol Biol 2005;347:683–91.
[28] Sharma P, Singh N, Sinha M, et al. Crystal structure of the peptidoglycan recognition protein at 1.8 Å resolution reveals dual strategy to combat infection through two independent functional homodimers. J Mol Biol 2008;378(4):923–32. https://doi.org/10.1016/j.jmb.2008.03.018.
[29] Leone P, Bischoff V, Kellenberger C, et al. Crystal structure of *Drosophila* PGRP-SD suggests binding to DAP-type but not lysine-type peptidoglycan. Mol Immunol 2008;45(9):2521–30. https://doi.org/10.1016/j.molimm.2008.01.015.
[30] Sahoo BR, Dubey PK, Goyal S, et al. Exploration of the binding modes of buffalo PGRP1 receptor complexed with meso-diaminopimelic acid and lysine-type peptidoglycan by molecular dynamics simulation and free energy calculation. Chem Biol Interact 2014;220:255–68. https://doi.org/10.1016/j.cbi.2014.06.028.